frontiers in Environmental Science

ORIGINAL RESEARCH
published: 18 October 2017
doi: 10.3389/fenvs.2017.00066

The Effect of WO_3 Modification of ZrO_2 Support on the Ni-Catalyzed Dry Reforming of Biogas Reaction for Syngas Production

*Nikolaos D. Charisiou[1], Georgios Siakavelas[1], Kyriakos N. Papageridis[1], Apostolos Baklavaridis[1], Lazaros Tzounis[2], Grammatiki Goula[3], Ioannis V. Yentekakis[3], Kyriaki Polychronopoulou[4] and Maria A. Goula[1]**

[1] Laboratory of Alternative Fuels and Environmental Catalysis, Department of Environmental and Pollution Control Engineering, Western Macedonia University of Applied Sciences, Kozani, Greece, [2] Composite and Smart Materials Laboratory, Department of Materials Science and Engineering, University of Ioannina, Ioannina, Greece, [3] Laboratory of Physical Chemistry and Chemical Processes, School of Environmental Engineering, Technical University of Crete, Crete, Greece, [4] Department of Mechanical Engineering, Khalifa University of Science and Technology, Abu Dhabi, United Arab Emirates

OPEN ACCESS

Edited by:
Yiu Fai Tsang, The Education University of Hong Kong, Hong Kong

Reviewed by:
Benjaram M. Reddy, Indian Institute of Chemical Technology (CSIR), India
Costas N. Costa, Cyprus University of Technology, Cyprus

***Correspondence:**
Maria A. Goula
mgoula@teiwm.gr

Specialty section:
This article was submitted to Wastewater Management, a section of the journal Frontiers in Environmental Science

Received: *20 June 2017*
Accepted: *29 September 2017*
Published: *18 October 2017*

Citation:
Charisiou ND, Siakavelas G, Papageridis KN, Baklavaridis A, Tzounis L, Goula G, Yentekakis IV, Polychronopoulou K and Goula MA (2017) The Effect of WO_3 Modification of ZrO_2 Support on the Ni-Catalyzed Dry Reforming of Biogas Reaction for Syngas Production. Front. Environ. Sci. 5:66. doi: 10.3389/fenvs.2017.00066

The time-on-stream catalytic performance and stability of 8 wt. % Ni catalyst supported on two commercially available catalytic supports, ZrO_2 and 15 wt.% WO_3-ZrO_2, was investigated under the biogas dry reforming reaction for syngas production, at 750°C and a biogas quality equal to $CH_4/CO_2 = 1.5$, that represents a common concentration of real biogas. A number of analytical techniques such as N_2 adsorption/desorption (BET method), XRD, H_2-TPR, NH_3- and CO_2-TPD, SEM, ICP, thermal analysis (TGA/DTG) and Raman spectroscopy were used in order to determine textural, structural and other physicochemical properties of the catalytic materials, and the type of carbon deposited on the catalytic surface of spent samples. These techniques were used in an attempt to understand better the effects of WO_3-induced modifications on the catalyst morphology, physicochemical properties and catalytic performance. Although Ni dispersion and reducibility characteristics were found superior on the modified Ni/WZr sample than that on Ni/Zr, its dry reforming of methane (DRM) performance was inferior; a result attributed to the enhanced acidity and complete loss of the basicity recorded on this catalyst, an effect that competes and finally overshadows the benefits of the other superior properties. Raman studies revealed that the degree of graphitization decreases with the insertion of WO_3 in the crystalline structure of the ZrO_2 support, as the I_D/I_G peak intensity ratio is 1.03 for the Ni/Zr and 1.29 for the Ni/WZr catalyst.

Keywords: biogas utilization, syngas production, zirconia, tungstated zirconia, dry reforming of methane, renewable carbon sources, cyclic economy

INTRODUCTION

It is widely accepted by the scientific community that mankind has approached a critical stage in its development where it must replace fossil fuels, its engine of growth for the past two centuries, with renewable energy technologies. This need is spurred on by the finite nature of fossil resources and the apocalyptic consequences on climate by the ever growing green house gas (GHG) emissions.

Synthesis gas (syngas), which at present is mainly being produced using natural or shale gas as feedstock, is a crucial intermediate resource for the petrochemical industry as it is necessary for the production of hydrogen, ammonia and Fischer-Tropsch liquid energy carriers, such as methanol, olefins, paraffins, aromatics and oxygenates. However, syngas can also be obtained via the dry reforming of methane (DRM) using biogas as feedstock, which has the attraction of utilizing CH_4 and CO_2, i.e., the most abundant greenhouse gases (Avraam et al., 2010; Martins et al., 2017; Yentekakis and Goula, 2017).

Although the stochiometry of the DRM (Equation 1) means that the ratio of H_2 to CO in the product stream is expected to be 1:1 (ideal for Fischer-Tropsch synthesis), the fact that the reverse water gas shift reaction (RWGS, Equation 2) also takes place simultaneously (consuming H_2), lowers this ratio. Carbon formation, which affects catalytic performance and H_2/CO product distribution, is induced by methane cracking (Equation 3) and the Boudouard reaction (Equation 4). Other reactions that may take place during the DRM include carbon gasification / oxidation and CO methanation (Kathiraser et al., 2015; Arbag et al., 2016; Charisiou et al., 2016a). As the overall reaction is strongly endothermic, it is usually operated at temperatures exceeding 650°C. In these conditions, methane cracking is favored, the RWGS is suppressed and the Boudouard reaction is thermodynamically inhibited (Goula et al., 2015; Mustu et al., 2016).

$$CH_4 + CO_2 \leftrightarrow 2CO + 2H_2 (\Delta H^{\circ}_{298} = +247 kJ/mol) \quad (1)$$

$$H_2 + CO_2 \leftrightarrow CO + H_2O (\Delta H^{\circ}_{298} = +41 kJ/mol) \quad (2)$$

$$CH_4 \leftrightarrow 2H_2 + C (\Delta H^{\circ}_{298} = +75 kJ/mol) \quad (3)$$

$$2CO \leftrightarrow CO_2 + C (\Delta H^{\circ}_{298} = -172 kJ/mol) \quad (4)$$

The major research challenge is the development of cheap catalysts that are resistant to both carbon formation and particle sintering. In this respect, nickel based catalysts attract particular attention as they are known to exhibit excellent catalytic performance; the drawback is that they suffer from the aforementioned problems (Goula et al., 2015; Charisiou et al., 2016b; Elsayed et al., 2017). In theory, coke deposition can be avoided by: (i) altering the electronic properties of metal-support interactions, (ii) influencing the size of metallic particles and, (iii) improving the oxygen storage capacity and mobility within supporting material (Roh et al., 2006; Kumar et al., 2007; Chen et al., 2008; Goula et al., 2014; Yentekakis et al., 2015, 2016; Han et al., 2017). Thus, the attempts that have been undertaken to improve the stability of DRM nickel catalysts have focused on the use of different oxides as supports (e.g., Al_2O_3, SiO_2, La_2O_3, CeO_2, ZrO_2) (Pompeo et al., 2007; Bereketidou and Goula, 2012; Li et al., 2016) or the use of a variety of dopants that include transition metals (e.g., Fe, Co, Sn) (Ay and Uner, 2015; Theofanidis et al., 2015; Zhao et al., 2016), noble metals (e.g., Ag, Pt, Pd, Ir) (Oemar et al., 2015; Yentekakis et al., 2015; Yu et al., 2015), lanthanide metals (e.g., La, Ce, Pr) (Goula et al., 2016a; Vasiliades et al., 2016; Xiang et al., 2016) and alkaline earth metals (e.g., Sr, Ca, Ba) (Bellido et al., 2009; Sutthiumporn and Kawi, 2011).

Although ZrO_2 is an oxide with a relatively low surface area, its notable thermal stability, strength and toughness, as well as, the fact that it is an acid-basic bi-functional oxide (as it contains both basic and acidic properties over its surface that have the capacity to work either independently or in cooperation), which has redox functions, makes it attractive for use in reforming reactions (Sarkar et al., 2007; Goula et al., 2017; Charisiou et al., in press).

Shiju et al. (2009) suggested that tungstated zirconia possesses mainly acid sites, but their number and strength is strongly depended on the preparation conditions chosen for the support and its calcination temperature. The same authors have also concluded that higher calcination temperatures can help the stabilization of the zirconia tetragonal phase and also anchor the WOx species on its surface. Macht and Iglesia (2008) reviewed the WO_3 dispersion phase evolution on zirconia, giving particular emphasis to the influence of the size and structural composition on catalytic performance. They concluded that the presence of oxygen-deficient domains contributed to poorly dispersed WO_x structures with low Brønsted acid site densities. On the other hand, Kourieh et al. (2012) observed higher Brønsted acidity on well dispersed WO_x domains over zirconia supports. In fact, tungstated zirconia represents a catalyst support that is already developed at the industrial level for paraffin isomerization (Baertsch et al., 2002; Zhou et al., 2009) however, to the best of our knowledge such catalysts have never been tested in the DRM reaction.

The purpose of the present study was to investigate the catalytic efficiency and time on steam stability of Ni dispersed on commercially available catalytic supports (ZrO_2 and WO_3-ZrO_2) for the dry DRM reaction. The catalysts were synthesized via the wet impregnation technique with a Ni loading of 8 wt.%. The temperature under investigation was 750°C (the common temperature used in methane reforming practical applications) and the CH_4/CO_2 ratio was equal to 1.5, simulating typical biogas quality.

The catalysts were characterized using techniques such as N_2 adsorption/desorption (BET method), X-Ray diffraction (XRD), temperature programmed reduction (H_2-TPR), temperature programmed desorption (NH_3- and CO_2-TPD), and inductively coupled plasma emission spectroscopy (ICP), in order to determine textural, structural and other physicochemical properties of the materials, particles' morphology and active phase loading. Scanning electron microscopy (SEM), thermal analysis (TGA/DTG) and Raman spectroscopy were used to help determine the amount and type of carbon deposited on the catalytic surface after exposure to DRM reaction conditions (spent samples).

MATERIALS AND METHODS

Catalyst Preparation

The supports used herein were kindly provided for free by Saint Gobain NorPro (**Table 1**). These were pelletized zirconia (labeled Zr) and tungsten – zirconia (WZr) oxides, which were crashed and sieved to 350–500 μm. The supports were then calcined at 800°C for 4 h. The catalysts were obtained via the wet impregnation technique using a $Ni(NO_3)_26H_2O$ (Sigma Aldrich) aqueous solution of concentration equal to 0.17M, in order

TABLE 1 | Properties of untreated catalyst carriers.

Support	ZrO_2	WO_3-ZrO_2
Size and shape	3.0 mm	3.0 mm
Packing density, Kg/m^3	*n/p*	1494
Median pore diameter, nm	*n/p*	16.1
SSA (m^2g^{-1})	77	116
Vp (mL g^{-1})	0.30	0.25
ZrO_2	*n/p*	83.5
HfO_2		1.5
WO_3		15
Phase	Monoclinic	Tetragonal

n/p, not provided.

to obtain catalysts with a Ni content of 8 wt.%. After water evaporation of the slurries under continuous stirring at 75°C for 5 h, suspensions were dried at 120°C for 12 h and calcined in air at 800°C for 4 h. These samples will be denoted herein as "calcined" catalysts. The samples were *in situ* activated for 1 h at 800°C under pure H_2 flow and will be denoted herein as "reduced" catalysts. The catalysts are labeled as Ni/Zr and Ni/WZr.

Catalyst Characterization

The total metal loading (wt.%) was determined using inductively coupled plasma atomic emission spectroscopy (ICP-AES) on a Perkin-Elmer Optima 4300DV apparatus. Additional information on samples preconditioning can be found in Goula et al. (2016b).

The 3Flex (Micromeritics, USA) accelerated surface area and porosimetry analyzer (equipped with three 0.1 Torr pressure transducers and a high-vacuum system) was used for obtaining N_2 adsorption/desorption isothermal curves at –196°C; measurements were recorded manometrically up to 1 bar. The multi-point Brunauer-Emmet-Teller (BET) method, in the relative pressure range $0.05 < P/P_0 < 0.20$, and the BJH theory were used for the calculation of total specific surface area (SSA) and pore size distribution (PSD), respectively. Additional information on samples preconditioning can be found in Charisiou et al. (2017).

The determination of the catalysts' crystalline structure was done by powder X-ray diffraction (PXRD), using a ThermoAl diffractometer at 40 kV and 30 mA, with Cu Kα radiation ($\lambda = 0.15178$ nm). Diffractograms were recorded in the $2\theta = 2$–70° range at a scanning rate of 0.04° 1.2 min^{-1}. The diffraction patterns were identified by comparison with those of known structure in the International Centre for Diffraction Data.

CO_2-temperature programmed desorption (TPD) and NH_3-TPD experiments were undertaken in an Autochem 2920, (Micromeritics, Atlanta, USA). Specifically, a gas mixture of 5 vol.% CO_2/Ar and 1 vol.% NH_3/He (30 NmL/min), was passed over ∼0.15 g of the catalysts (20 vol.% O_2/He, 500°C, 2 h) using a temperature ramp of 30°C/min and the TCD signal was continuously recorded. Temperature programmed reduction (H_2-TPR) was performed by loading 100 mg of the calcined catalysts or supports in a U-type quartz tube adapted to a continuous flow TPR/TPD apparatus coupled with mass spectrometry, following the procedures described in detail elsewhere (Yentekakis et al., 2016).

Morphological examination of fresh and used catalysts was undertaken by SEM in a JEOL 6610LV. The elemental analysis, using Energy Dispersive Spectroscopy (EDS), was carried with the use of a large area (80 mm^2) silicon drift detector (X-Max 80 Oxford Instruments). The acquisition and analysis of images, elements maps and spectra was done using the AZtech Nanoanalysis software (Oxford Instruments) following the methodology described previously (Charisiou et al., 2017).

A thermogravimetric analyzer (Leco TGA701) was used for measuring the amount of carbon deposited on the catalysts. The thermal decomposition process of the coke formed onto the spent catalysts was also obtained. In the procedure, 50 mg of the spent catalyst were subjected to TGA scan from room temperature (RT) to 1,000°C at a heating rate of 10°C min^{-1} under a flow of dry air (3.5 L min^{-1}). Curie point standards were utilized for the temperature calibration.

The coke deposited on the spent catalytic samples was also characterized by Raman spectroscopy. The equipment and methodology employed have been described in a previous publication (Papageridis et al., 2016). In brief, the spectra were collected with the use of a WITEC alpha300R micro-Raman system (RAMAN Imaging System WITEC alpha300R) with a 20× long distance objective (0.35 numerical aperture) in the back-scattering geometry with an excitation wavelength of 532 nm from an Ar^+ ion laser (laser power set at 2 mW calibrated against a silicon standard).

Catalytic Tests

The catalytic tests were undertaken at atmospheric pressure, using a continuous flow, fixed bed, tubular reactor. The gas mixture used as feed in the reactor inlet had a total flow rate of 100 mL min^{-1} and consisted of v/v 30%CH_4/20%CO_2/50%He. This corresponds to a CH_4 /CO_2 molar ratio equal to 1.5 and a Weight-basis Hourly Space Velocity (WHSV) of 120,000 mL g^{-1} h^{-1}.

The catalysts were activated by *in situ* reduction under hydrogen flow (100 mL min^{-1}) at 800°C for 1 h. Following activation, the reactor was returned to the temperature of interest under He flow (100 mL min^{-1}).

The experimental protocol followed was designed with the purpose of investigating time-on-stream catalytic stability and carbon deposition at typical temperatures found in practical applications in biogas utilization processes, i.e., at 750°C. Tests lasted for a sufficiently long time-on-stream equal to 28 h.

The gaseous reaction products were analyzed by on-line gas chromatography in a CG-Agilent 7890A gas chromatograph. The instrument was equipped with two parallel columns, HP-Plot-Q (19095-Q04, 30 m length, 0.530 mm I.D.) and HP-Molesieve (19095P-MSO, 30 m length, 0.530 mm I.D.), and with TCD and FID detectors.

Methane or carbon dioxide conversions, hydrogen or carbon monoxide yields and H_2/CO molar ratio were determined

according to the following equations:

$$X_{CH_4}\,(\%) = \frac{F_{CH_4,in} - F_{CH_4,out}}{F_{CH_4,in}} \times 100 \quad (5)$$

$$X_{CO_2}\,(\%) = \frac{F_{CO_2,in} - F_{CO_2,out}}{F_{CO_2,in}} \times 100 \quad (6)$$

$$Y_{H_2}\,(\%) = \frac{F_{H_2}}{2F_{CH_4,in}} \times 100 \quad (7)$$

$$Y_{CO}\,(\%) = \frac{F_{CO}}{F_{CH_4,in} + F_{CO_2,in}} \times 100 \quad (8)$$

$$Molar\,ratio = \frac{F_{H_2,out}}{F_{CO,out}} \quad (9)$$

where $F_{i,in}$ or $F_{i,out}$ is the flow rate of the component i in feed or effluent gas mixture.

RESULTS AND DISCUSSION

Characterization Results

Textural and Structural Characterization

The ICP results presented in **Table 2** show that the desired active phase loading was achieved for both catalysts. **Table 2** also shows the SSA of the calcined samples and as can be observed, the catalyst based on the modified zirconia support (Ni/WZr) exhibits a lower SSA value, namely 16 m^2g^{-1}, in comparison to the one supported on unmodified zirconia (Ni/Zr = 44 m^2g^{-1}). The SSA values of both catalysts (**Table 2**) are much lower to that of the commercially provided supporting materials (**Table 1**), but notably this drop is more noticeable for the Ni/WZr sample. This can be explained by the high temperature at which the supports were initially calcined (800°C), which was also expected to bring about a transformation of their crystalline phases (as will be shown below when discussing the XRD results). Moreover, a partial pore blockage by nickel particle species deposited over the supports' surface during catalyst preparation is also likely (Goula et al., 2015, 2016b). In addition, Chai et al. (2017) have reported that at high calcination temperatures the SSA of tungstated zirconia declines due to the sintering of ZrO_2, which is also accompanied by a significant rise in the tungsten surface density.

The N_2 adsorption-desorption isotherms at −196°C of the reduced catalysts are shown in **Figure 1**; their corresponding PSD characteristics are presented as insets. For the Ni/Zr catalyst the isotherm is IV-type and has H4-type hysteresis. Moreover, its PSD shows that the majority of pore population are found in the meso-range (Sing et al., 1985). In addition, it is clear that the distribution of pore sizes is in agreement with the hysteresis loop shape. Moreover, some ordering in the porosity of the Ni/Zr catalyst can be inferred based on the hysteresis shape. In contrast, the Ni/WZr sample exhibits a Type II isotherm, which is more typical of mesoporous materials with some microporosity. This means that minor adsorption is observed at the low pressure regime ($P/P_0 < 0.05$) and major adsorption at the high pressure regime ($0.7 < P/P_0 < 1.0$) (Rouquerol et al., 1999). A small hysteresis loop (H2-type) was also observed, as the N_2 desorption rate was lower than its adsorption one (attributed to percolation effects on porous media).

TABLE 2 | Physicochemical characterization results for the reduced Ni/Zr and Ni/WZr catalysts.

Catalyst	Metal loading (Ni, wt. %)	SSA (m^2g^{-1})	Pore volume (cm^3g^{-1})	Av. pore diameter (nm)	Ni^0 mean crystallite size (nm)[a]	Ni^0 dispersion (%)[b]
Ni/Zr	7.65	44	0.05	19.9	23.0	2.9
Ni/WZr	8.08	16	0.15	16.6	11.5	5.7

[a] *Evaluated by Scherrer analysis of the XRD findings.*
[b] *Calculated by the Vannice method (Luisetto et al., 2015).*

Results from X-ray diffraction analysis of the calcined supports and calcined/reduced catalysts are presented in **Figure 2**. In general, zirconium oxide (ZrO_2) can exhibit cubic, tetragonal and monoclinic polymorphs however, as is well understood, the transformation from one form to another depends not only on temperature, but also to the existence of impurities, which are usual in natural ores (e.g., Hf, Si, Fe) (Teterycz et al., 2003). It is pointed out that impurities were also present in the materials used as supports herein (**Table 1**). According to the available literature, the tetragonal ZrO_2 appears at $2\theta \approx 30.0°$, 33.9°, 34.8°, 35.1° 49.4°, 50.0°, 58.27°, 59.37°, and 62.8°, the monoclinic ZrO_2 appears at $2\theta \approx 24.0°$, 28.2°, 31.5°, 34.2°, 34.4°, 35.3°, and 40.7° and cubic ZrO_2 appears at $2\theta \approx 30.5°$, 50.5°, and 60.4° (Titus et al., 2016). It is also noted that the XRD reflections of cubic and tetragonal structures are very close, which makes it difficult to differentiate between them (Iriondo et al., 2012). Moreover, literature reports suggest that during calcination, surface species in WO_3-ZrO_2 can be removed, which can lead to the simultaneous existence of reduced and oxidized W atoms (W^{5+}, W^{6+}) (Yori et al., 1999). This could in turn lead to the creation of anionic vacancies and to the stabilization of the tetragonal zirconia habitat. At high calcination temperatures, surface W^{5+} can be oxidized to W^{6+} and the former structure can become unstable. As a result, tungsten may sinter into larger WO_3 particles and zirconia can be transformed to the monoclinic phase (Busto et al., 2010); the latter was also evidenced in our case. The diffractograms of the calcined catalysts also show the existence of NiO phases, which can be attributed to (111) and (200) of the cubic lattice plane (peaks at $2\theta = 37.2°$ and 43.2°). In contrast, NiO was not detected on the reduced samples however, a peak corresponding to metallic nickel (Ni^0) at $2\theta = 44.5°$ was visible in the diffractograms. Moreover, the fact that the crystalline WO_3 phase ($2\theta = 23.2°$, 23.7°, and 24.3°) was not detected in either the calcined or reduced sample is an indication that tungsten was highly incorporated and dispersed into the ZrO_2 lattice, not providing individual WO_3 particles (Busto et al., 2010).

The Ni^0 species mean particle size was determined form the XRD spectra using Scherrer analysis in order to estimate the Ni dispersion (D_{Ni}) values of the reduced samples (Luisetto et al., 2015). The nickel crystallite size and the corresponding dispersion values for the Ni/Zr and Ni/WZr samples were 23.0 nm, 2.9% and 11.5 nm, 5.7%, respectively (**Table 2**). The origin of these differences can be attributed to the existence

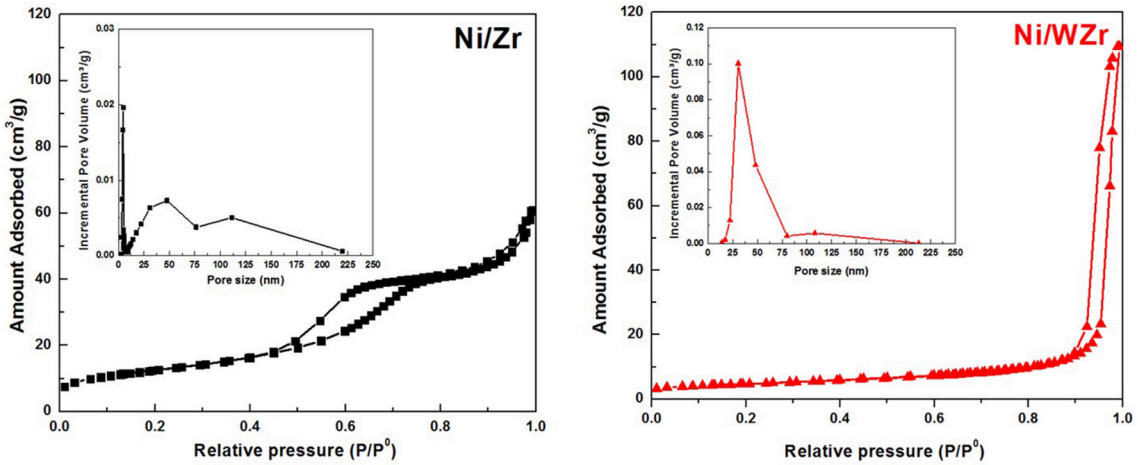

FIGURE 1 | N_2 adsorption-desorption isotherms and pore size distribution (inset) of the catalysts.

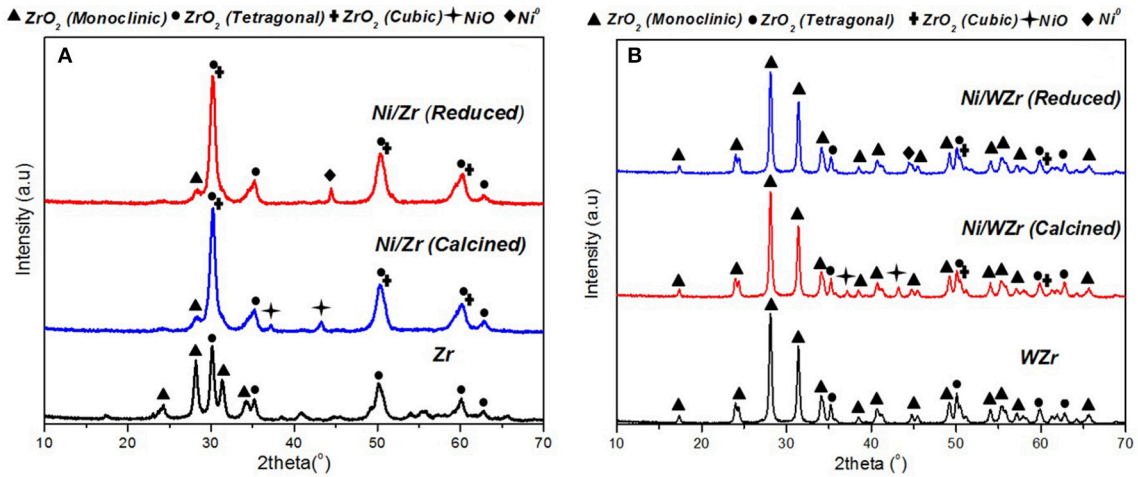

FIGURE 2 | XRD patterns of calcined supports and calcined and reduced samples: **(A)** Ni/Zr, **(B)** Ni/WZr ($\lambda = 0.154178$ nm, $2\theta = 2$–$70°$, Scanning rate: 0.04° over 1.2 min^{-1}).

of higher concentration of anionic defects on m-ZrO_2 than on t-ZrO_2. The different symmetry and spacing of the OH and Zr-O bonds at tetragonal ZrO_2 and monoclinic ZrO_2 can play an important role in the dispersion of the active metal component and consequently on the properties of the catalytic systems (Chai et al., 2017; Silveira et al., 2017). Sato et al. (2013) investigating the effect of the ZrO_2 phase on the structure and behavior of supported Cu catalysts for ethanol conversion, concluded that the activity of Cu/ZrO_2 catalysts is strongly dependent on the phase structure of ZrO_2, as Cu catalysts supported over monoclinic ZrO_2 were found more active than catalysts with the same Cu surface density deposited on tetragonal ZrO_2. Rhodes and Bell (2005) have also shown that the tetragonal and monoclinic modifications of ZrO_2 possess different acid/base properties and surface hydroxyl group concentrations.

Surface Acidity and Basicity

The number and strength of acid sites present in the catalysts tested herein was examined using NH_3-TPD. Depending on the desorption temperature of NH_3, acid sites can be classified into weak (<200°C), medium (200–350°C), strong (350–600°C) and very strong (>600°C) (Sundaramurthy et al., 2008). As shown in **Figure 3A**, the main desorption temperature peaks of the Ni/Zr catalyst were found at >435°C (**Figure 3A**), indicating that this sample has mainly strong to very strong acid sites; small peaks at the lower temperature range are also apparent. According to Damyanova et al. (1997) the acidic character of the ZrO_2 is mainly attributed to Lewis acid sites, mainly because of the greater ionic character of the Zr-O bond. For the Ni/WZr catalyst the appearance of a high and broad peak at the low to medium desorption temperature range is an indication that the addition of WO_3 to ZrO_3 introduces additional strong Brönsted

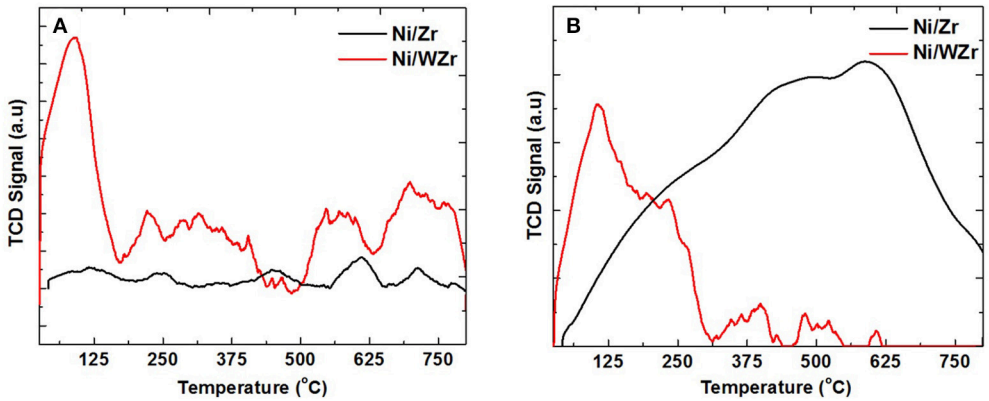

FIGURE 3 | (A) NH_3-TPD and **(B)** CO_2-TPD, for both Ni/Zr and Ni/WZr catalysts (Catalyst mass: 0.15 g, Gas mixture: 5 vol % CO_2/Ar and 1 vol.% NH_3/He, Gas flow rate: 30 NmL/min, Temperature ramp of 30 °C/min).

acid sites. This is in agreement with Phung et al. (2015), reporting evidence for the presence of both Lewis and Brönsted acid sites on WO_3/ZrO_2 samples. It is noted that Busto et al. (2008) suggested that the relative proportion of strong acid sites for tungstated zirconia samples calcined at 800°C, as in our case, could be as high as ∼40%. The absence of W-related phase in the XRD results, points to a substantial incorporation of tungsten atoms into the zirconia lattice and thus, to an extended interaction with the ZrO_2 phase, which in turn affects in high degree the ionic character of the Zr-O bonds, giving rise to the increased acidity observed.

The number and strength of basic sites present in the catalysts tested herein was examined using CO_2-TPD (**Figure 3B**). The basic sites can be classified according to their strength related to the CO_2 temperature desorption peaks as weak (50–200°C), intermediate (200–400°C), strong (400–650°C) and very strong (>650°C). This is because the CO_2 adsorbed on the weaker basic sites is desorbed at relatively low temperature, while the CO_2 adsorbed on the stronger sites is desorbed at somewhat high temperature (Fakeeha et al., 2014). Typically, for solid oxides the basic sites can be attributed to: (i) weak associated with weak Brønsted OH groups, (ii) medium strength metal-oxygen Lewis pairs and (iii) strong Lewis basic sites associated with oxygen anions (Debecker et al., 2009; Gac, 2011). For the Ni/Zr catalyst a broad CO_2 desorption peak can be seen, which is more predominant in the medium and high temperature (multiple peaks underneath at 250, 420, and 620°C can be seen). For the Ni/WZr on the other hand, the CO_2-TPD peak is broad at temperatures lower than 300°C; this can be linked to the existence of weaker basic sites on the W-modified surface compared to the unmodified one.

As reported in the literature, the DRM performance can be correlated with the number and strength of acid/basic sites as the adsorption of CO_2 during the reaction can supply additional species of surface oxygen on the surface of the catalyst and facilitate the gasification of the intermediate carbonaceous species. As a matter of fact, the acid/basic properties of catalysts are considered one of the crucial factors that can significantly affect the DRM catalytic behavior; others include the active phase size (i.e., dispersion), textural characteristics, carbon deposition and morphology and the strength of metal-support interactions.

Temperature Programmed Reduction (H_2-TPR)

The catalysts' reducibility and the strength of interaction between Ni species and the surface of the supporting materials were investigated by H_2-TPR experiments (**Figure 4**). The Gaussian-type deconvolution of the profiles is also being presented for both catalytic samples. Clearly, the Ni/Zr catalyst exhibits three broad peaks; (a) the lowest peak is found between 450 to 480°C, (b) the peak in the middle is found around 620°C and, (c) the higher peak found around 730°C. The first two peaks can be related to the reduction of Ni^{2+} species interacting with ZrO_2, while the high reduction temperature peak likely corresponds to the reduction of NiO-ZrO_2 solid solutions. Specifically, using the deconvolution profile of the Ni/Zr catalyst, it is evidenced that the low temperature reduction peak is formed by the sum of two peaks formed at 442 and at 495°C, respectively. The former may be attributed to Ni^{2+} species interacting with tetragonal zirconia and the latter, to Ni^{2+} species interacting with cubic zirconia (Goula et al., 2016a). The sum of the two reduction peaks (567 and 609°C) forming the middle temperature peak can be associated with Ni^{2+} species bound to monoclinic zirconia (Youn et al., 2009). In regards to the Ni/WZr catalyst, only two peaks can be detected; the first is found at low (350–500°C) and the second at higher (500–700°C) temperatures. It can be also seen that, the low temperature peak can be deconvoluted in two peaks (423 and 460°C) and the high temperature peak into three peaks (528, 600, and 648°C), confirming the existence of nickel species having different strength of interaction with the support (Torres et al., 2012). An additional observation is the absence of peaks at high temperatures (T>700°C), indicating the absence of possible NiO-ZrO_2 solid solutions. Moreover, the broadening of the peak at temperatures between 500 and 700°C is due to the enrichment of the support in monoclinic zirconia crystal phase (as also shown by the XRD results). Thus, it can be concluded that the Ni/WZr catalyst is easier to reduce in comparison to the Ni/Zr.

Carbon Analysis

The morphology of the carbonaceous material that was formed over the surface of the spent catalysts was examined by SEM (**Figure 5**). The images reveal that carbon nano fibers (CNFs) and/or carbon nano tubes (CNTs) have grown on the Ni/Zr sample with an average rate equal to 1.86 μmol C/h (as determined by TGA/DTG; see below) and it is possible to suggest that they are randomly oriented in accordance with the directions preferred by the crystals of the catalysts that are needed for growing the carbon nano-structures. The average carbon formation rate on Ni/WZr catalyst was 1.11 μmol C/h and some carbon filaments can also be seen on this sample, but these are harder to spot, fewer in number and appear much shorter in comparison. Carbon mapping of this initial examination shows that carbon is more or less evenly spread throughout the entire surface of the spent catalytic samples.

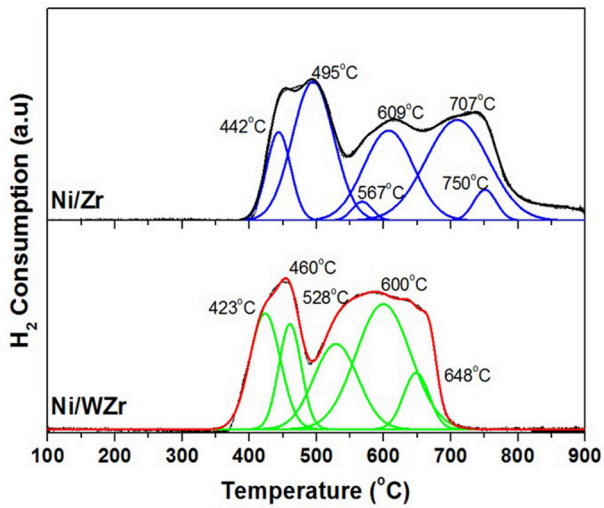

FIGURE 4 | TPR profiles of both catalysts (Catalyst mass: 100 mg, Total flow: 16 mL min^{-1} (1% (v/v) H_2 in He). Temperature: RT-950°C, Ramp rate: 10°C min^{-1}, Main m/z fragment: $H_2 = 2$).

TGA/DTG analysis was also performed on the carbonaceous material deposited on the surface of the spent catalysts. Literature reports that amorphous carbon combusts in the temperature range of 200–500°C, structures with disorders, such as CNFs and/or CNTs containing a small number of defects combust between 500 and 600°C, while more graphitic structures such as multi walled (MW) CNTs are burned between 600 and 750°C (Velasquez et al., 2014). The DTG results presented in **Figure 6** are in agreement with the SEM findings discussed above, as the peak corresponding to the Ni/Zr catalyst is slightly shifted to higher temperatures in comparison to the Ni/WZr sample.

The spent catalysts were additionally examined by Raman spectroscopy (**Figure 7**); the aim was to get a better understanding regarding the nature and the graphitization order characteristics of the carbon deposits formed onto the spent catalysts. Both samples, after spectra deconvolution, show clearly the existence of the D, G, 2D, G+D and 2D'-bands (at 1,345, 1,565, 2,675, 2,900, and 3,210 cm^{-1}, respectively); the D"-band (located at 2,435 cm^{-1}) can only be observed on the Ni/WZr sample. The location of the G and D-band signals suggest the formation of CNTs (Lehman et al., 2011), while the detection of the 2D-band indicates that these are MWCNT (Ferreira et al., 2010). The relative intensity of the D and G bands (I_D/I_G) is a good indicator of the degree of crystallinity of the carbon formed during the reforming reaction, as smaller I_D/I_G values point to higher crystallinity due to the larger presence of the graphitized carbon formed (Zhao et al., 2011). For the catalysts tested herein, it is clear that the degree of graphitization decreases with the insertion of WO_3 in the crystalline structure of the ZrO_2 support,

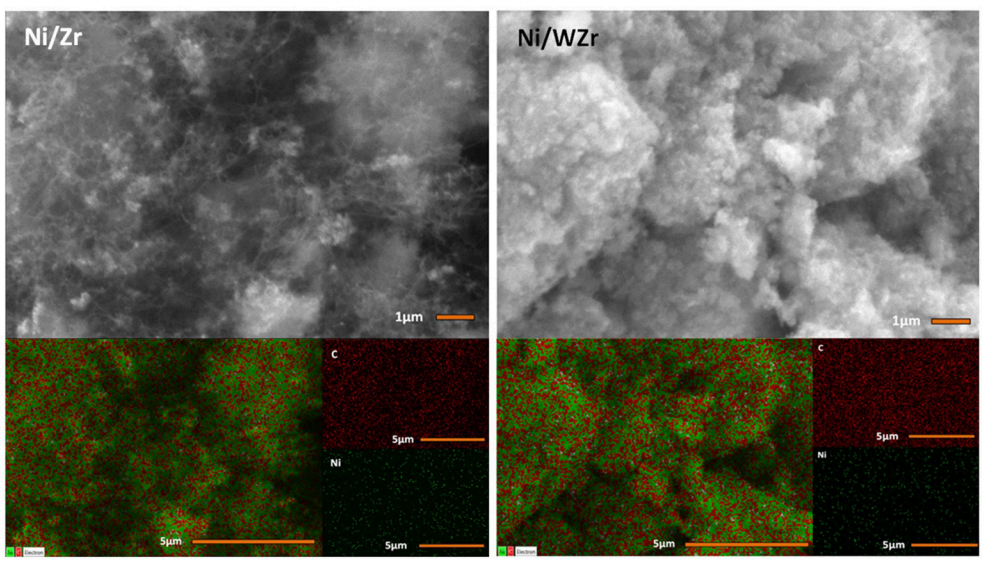

FIGURE 5 | SEM images and carbon mapping of spent catalysts.

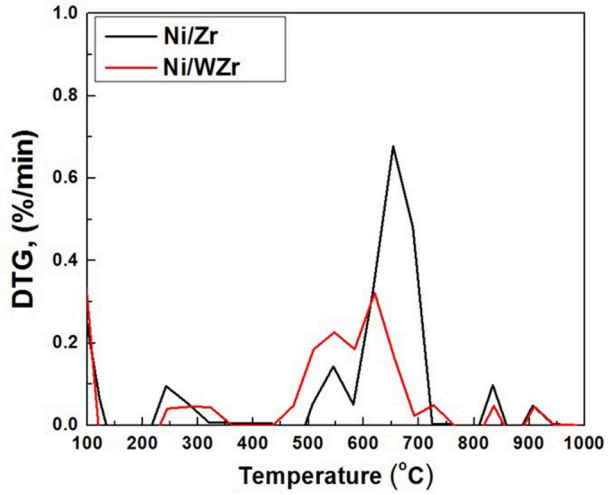

FIGURE 6 | DTG graphs of the spent catalysts.

as the I_D/I_G peak intensity ratio is 1.03 for the Ni/Zr and 1.29 for the Ni/WZr, in good agreement with the SEM and DTG results presented above. The presence of the D″ band on the Ni/WZr catalyst indicates that defects have been inserted in the carbon lattice of the MWCNT during the catalytic reaction (Kaniyoor and Ramaprabhu, 2012; Tsirka et al., 2017).

Catalytic Performance

It is widely accepted in the literature that during the dry DRM, the main reaction (Equation 1) is accompanied by competing parallel reactions that modify the DRM stoichiometry (products distribution), such as the reverse water gas shift (Equation 2), methane cracking (Equation 3) and the Boudouard reaction (Equation 4) (Usman et al., 2015; Atashi et al., 2017). Regarding carbon, it is generally accepted that its formation decreases with increasing temperature (carbon formation is thermodynamically favored at lower temperatures), however considerable amounts are formed even at temperatures as high as 800°C (Nikoo and Amin, 2011; Jafarbegloo et al., 2015). It should also be noted that large metal ensembles stimulate coke formation (Bawadi et al., 2017).

In **Figure 8** the transient, time-on-stream variations of the DRM performance i.e., CH_4 and CO_2 conversions, H_2 and CO yields, and H_2/CO molar ratio, at a constant temperature of 750°C typically encountered in practical methane reforming processes, are depicted for both catalysts. Although the initial (at $t = 0$) performance characteristics of the Ni/Zr and Ni/WZr catalysts are quite close, a progressive drop in activity is evidenced for both catalysts; however this is more pronounced for the tungstated zirconia supported sample (Ni/WZr). Specifically, for the Ni/Zr catalyst, the reactants' conversions record values from 52 to 22% for CH_4 and from 77 to 42% for CO_2. The same stands for products' yield, with Y_{H2} and Y_{CO} values dropping from 42 to18% and from 55 to 36%, respectively. For the Ni/WZr catalyst, CH_4 and CO_2 conversion values decrease from 47 to 11% and from 68 to 22%, respectively. A descending trend can be also observed for the H_2 and CO yield with values ranging from 42 to 16% and 50 to 25%, respectively. Since the yields of H_2 and CO as well as the conversion of CO_2 are also influenced by the reverse WGS and Boudouard reactions, the conversion of CH_4 can stand as the most meaningful parameter to analyze the DRM transient performance (Sokolov et al., 2013). According to $\Delta X_{(CH4)}$ (%) $= 100[(X_{CH4init}\text{-}X_{CH4final})/X_{CH4init}]$ this loss was estimated as 60% for the Ni/Zr and 77% for the Ni/WZr catalyst, indicating a higher deactivation rate for the latter system during the time-on-stream experiments.

In a first approximation, and taking into account the higher population of Ni active cites per gram of catalyst on the modified Ni/WZr catalyst in comparison to that on Ni/Zr (dispersion 5.7 vs. 2.9%, respectively; **Table 1**), a better DRM behavior of the modified catalyst would have been expected, at least at the beginning of the transient experiments shown in **Figure 8**. As is widely accepted in the literature, smaller-sized nickel metal precursors can help provide higher catalytic activity and stability and suppress carbon deposition (Usman et al., 2015; Bawadi et al., 2017). As an example, Han et al. (2017) evaluated the dependence of the CH_4 or CO_2 turnover frequency on the Ni size and showed that Ni nano-particles of 2.6 nm had 4.1 times higher methane turnover frequency in comparison to Ni nano-particles with a size of 17.3 nm. The decrease in turnover frequency was reduced as the size of the Ni nano-particles increased. However, this here is not the case as other factors rather than dispersion seems to affect more profoundly catalytic performance. The enhanced acidity for all kinds of acid sites (from weak up to very strong; **Figure 3A**), together with the complete loss of the medium and strong basic sites, found for the Ni/WZr catalyst (**Figure 3B**), are most probably the origin of this aberration. Literature data are in agreement with this view; it has been well established that enhanced bacisity of the catalysts promotes the CO_2 activation (dissociative adsorption) and thus DRM performance (Bitter et al., 1997; Rezaei et al., 2008), whilst the opposite is true on catalysts with enhanced acidity (Ni et al., 2012; Lovell et al., 2014). The slightly enhanced reducibility of the Ni/WZr catalyst in comparison to that of Ni/Zr, indicated by the H_2-TPR experiments in **Figure 4**, expected to act positively on DRM performance, seems also to have a marginal effect on DRM behavior in comparison to the adverse effect of acidity.

Moreover, the higher deactivation rate under passing of time for the modified Ni/WZr catalyst can be attributed to carbon deposition phenomena, in combination to the smaller mean pore size diameter of this catalyst (**Table 1**) Thus, under the relatively close characteristics of the carbon deposition phenomena (similar deposition rates and kinds of carbon formed), the smaller (and narrower) PSD of Ni/WZr, further aggravated by the lower SSA values, can be reasonably expected to be more prone to pores blocking phenomena, and thus catalytic performance degradation.

It can be also seen that the H_2/CO molar ratio (**Figure 8C**), also decreases with reaction time starting at about unity for both catalysts and reaching the value of 0.6 for the Ni/Zr and 0.8 for the Ni/WZr one. This observation could be of importance as

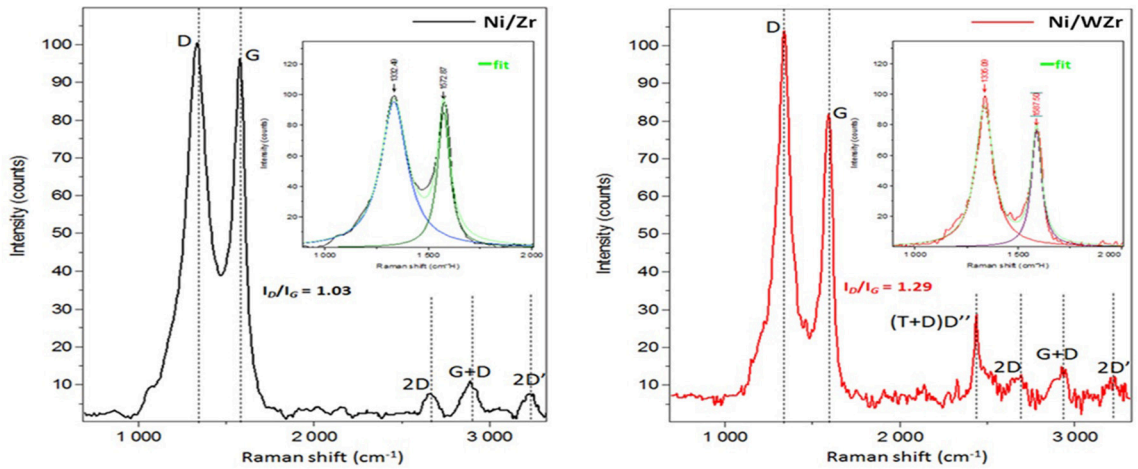

FIGURE 7 | Raman spectra of spend catalysts after the deconvolution process to yield Lorentzian D-peak, G-peak and D' peak (inset, the first order region of the spectra).

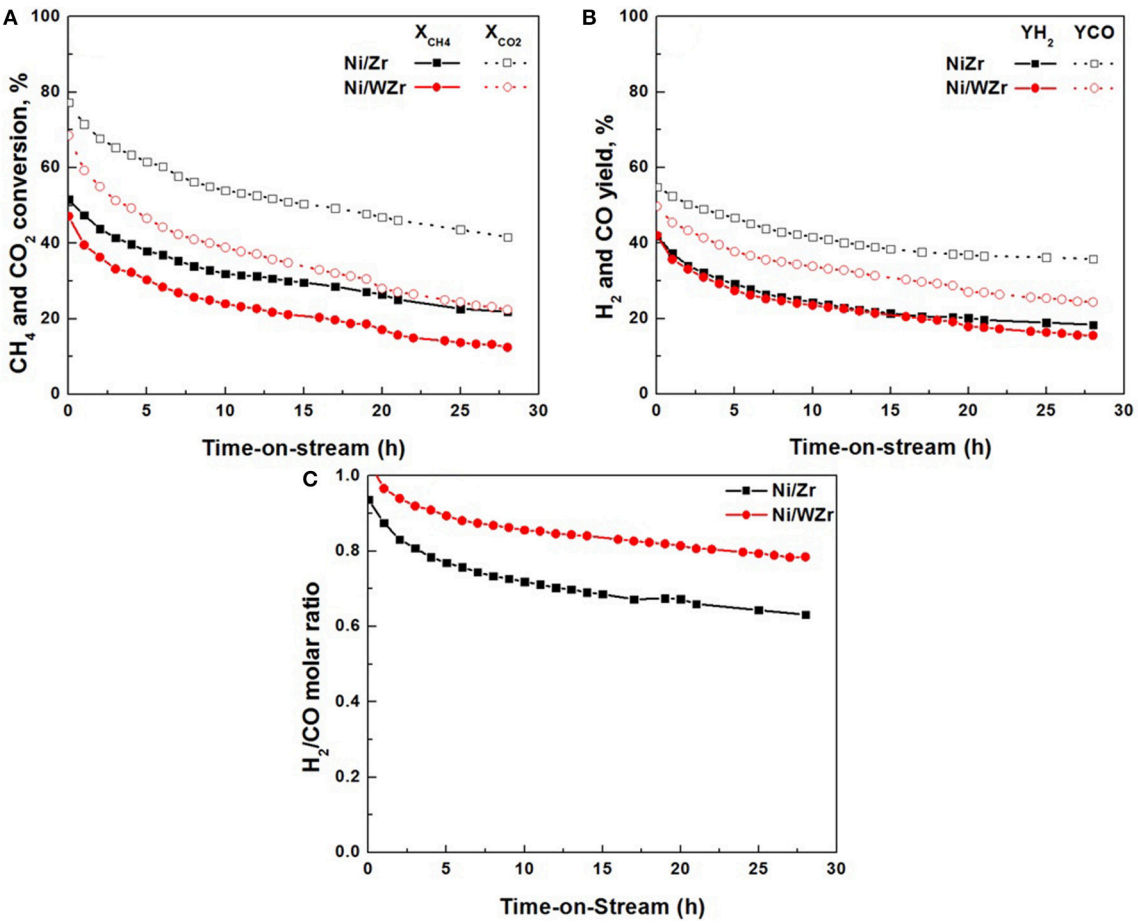

FIGURE 8 | Time-on-stream catalytic performance and stability of Ni/Zr and Ni/WZr catalysts at 750°C: **(A)** CH_4 and CO_2 conversions, **(B)** H_2 and CO yields, %, **(C)** H_2/CO molar ratio; Reaction conditions: Total feed flow rate of 100 mL min^{-1} (30%CH_4/20%CO_2/50%He).

H_2/CO values have a specific meaning on the trend of the system to form carbon (Challiwala et al., 2017). It has been reported that carbon deposition on the catalytic surface can occur as a result of the disproportionation of CO in the Boudouard reaction (Equation 4) or the methane cracking (Equation 3) over metallic Ni sites. It has also been suggested that the reverse Boudouard reaction (Equation 4) can help oxidize carbon deposits to CO by gaseous CO_2. Moreover, carbon deposits can be oxidized to CO_2 by the surface oxygen of the support ($C + O_2 \rightarrow CO_2$) (Gonzalez-DelaCruz et al., 2010; Damyanova et al., 2012; Sokolov et al., 2012; Taufiq-Yap et al., 2013). Even though the mechanism of the DRM process has been widely studied, the overall reaction scheme, as well as the rate determining step, have not been considered similar in all reports; these depend on the reaction conditions, the supporting materials and the active phase used (Bradford and Vannice, 1998; Bachiller-Baeza et al., 2013; Bobin et al., 2013). It is generally accepted that methane is activated on the surface of metal, while CO_2 can be activated either on the support (Damyanova et al., 2009), or at the metal-support interstitial sites (Sokolov et al., 2013), or even on the metal surface (Bachiller-Baeza et al., 2013; Bobin et al., 2013). Consequently, the surface CHx fragments or the surface C species derived from methane dissociation react with active O or OH species and desorbs as CO and H_2 products (Chen et al., 2002). Therefore, activation/ dissociation of methane on the active metal surface is a key reaction step that has been claimed to be irreversible in some cases (Wei and Iglesia, 2004; Bobin et al., 2013) and reversible in others (Bradford and Vannice, 1998; Yamaguchi and Iglesia, 2010). If the as formed carbon cannot be effectively gasified, coke deposition takes place and CNTs or graphite layers surrounding the metal particles can be formed. The enhanced H_2/CO values on the Ni/WZr catalyst in the present study, as a result of a reduced CO yield performance (**Figure 8B**) implies a depress on the CO_2 activation and therefore on the reactions related to CO formation (reverse Boudouard, water gas shift), which are in accord to our consideration regarding the adverse effect of the enhanced acidity of Ni/WZr catalyst.

CONCLUSIONS

WO_3 incorporation into ZrO_2 can induce improvements on the dispersion and reducibility of Ni particles deposited on this modified support (Ni/WZr). It also provides a typical mesoporous material with a narrow PSD, but with a lower surface area in comparison to its unmodified counterpart Ni/Zr. On the other hand the modified Ni/WZr material obeys enhanced acidity and complete absence of the medium and strong basicity in comparison to the unmodified Ni/Zr.

These factors are in competition during the dry DRM reaction, under which the modified Ni/WZr catalyst appears inferior in performance compared to Ni/Zr, as a result of its enhanced acidity, which seems to overgrow any positive effects expected from the better dispersion and reducibility of this material.

Average carbon deposition rate after 28 h of operation on DRM, was higher on the Ni/Zr catalyst (due to the larger metal ensembles on this catalyst, which stimulate coke formation), but the time-on-stream stability was better to that of Ni/WZr. This is attributed to the higher average PSD and the larger surface area of Ni/Zr vs. Ni/WZr, factors that both reduce the possibility of pores blocking and thus the deterioration of catalyst performance due to carbon deposition. Most of the carbon found on spent Ni/Zr and Ni/WZr catalysts was in both cases graphitic, i.e., the kind of carbon which has high trend for accumulation due to its low reactivity with surface oxygen species.

AUTHOR CONTRIBUTIONS

NC designed the experimental work and contributed to the write up of the manuscript. GS performed the experimental work regarding catalytic testing. KNP performed the TGA experiments. AB performed the SEM experiments. LT performed the Raman experiments. GG performed the TPR experiments. IY contributed to the write up of the manuscript. KP performed the BET and TPD experiments. MG had overall responsibility of the experimental work and contributed and supervised the write up of the manuscript.

REFERENCES

Arbag, H., Yasyerli, S., Yasyerli, N., Dogu, G., and Dogu, T. (2016). Enhancement of catalytic performance of Ni based mesoporous alumina by Co incorporation in conversion of biogas to synthesis gas. *Appl. Catal. B* 198, 245–265. doi: 10.1016/j.apcatb.2016.05.064

Atashi, H., Gholizadeh, J., Tabrizi, F. F., Tayebi, J., and Mousavi, S. A. H. S. (2017). Thermodynamic analysis of carbon dioxide reforming of methane to syngas with statistical methods. *Int. J. Hydrogen Energy* 42, 5464–5471. doi: 10.1016/j.ijhydene.2016.07.184

Avraam, D. G., Halkides, T. I., Liguras, D. K., Bereketidou, O. A., and Goula, M. A. (2010). An experimental and theoretical approach for the biogas steam reforming reaction. *Int. J. Hydrogen Energy* 35, 9818–9827. doi: 10.1016/j.ijhydene.2010.05.106

Ay, H., and Uner, D. (2015). Dry reforming of methane over CeO2 supported Ni, Co and Ni-Co catalysts. *Appl. Catal. B* 197, 128–138. doi: 10.1016/j.apcatb.2015.05.013

Bachiller-Baeza, B., Mateos-Pedrero, C., Soria, M. A., Guerrero-Ruiz, A., Rodemerck, U., and Rodriguez-Ramos, I. R. (2013). Transient studies of low-temperature dry reforming of methane over Ni-CaO/ZrO_2-La_2O_3. *Appl. Catal. B* 129, 450–459. doi: 10.1016/j.apcatb.2012.09.052

Baertsch, C. D., Komala, K. T., Chua, Y.-H., and Iglesia, E. (2002). Genesis of Bronsted acid sites during dehydration of 2-butanol on tungsten oxide catalysts. *J. Catal.* 205, 44–57. doi: 10.1006/jcat.2001.3426

Bawadi, A., Nur Azeanni, A. G., and Dai-Viet, N. V. (2017). Recent advances in dry reforming of methane over Ni-based catalysts. *J. Cleaner Prod.* 162, 170–185. doi: 10.1016/j.jclepro.2017.05.176

Bellido, J. D. A., De Souza, J. E., M'Peko, J. C., and Assaf, E. M. (2009). Effect of adding CaO to ZrO_2 support on nickel catalyst activity in dry reforming of methane. *Appl. Catal. A* 358, 215–223. doi: 10.1016/j.apcata.2009.02.014

Bereketidou, O. A., and Goula, M. A. (2012). Biogas reforming for syngas production over nickel supported on ceria-alumina catalysts. *Catal. Today* 195, 93–100. doi: 10.1016/j.cattod.2012.07.006

Bitter, J. H., Seshan, K., and Lercher, J. A. (1997). The state of zirconia supported platinum catalysts for CO_2/CH_4 reforming. *J. Catal.* 171, 279–286. doi: 10.1006/jcat.1997.1792

Bobin, A. S., Sadykov, V. A., Rogov, V. A., Mezentseva, N. V., Alikina, G. M., Sadovskaya, E. M., et al. (2013). Mechanism of CH_4 dry reforming on nanocrystalline doped Ceria-Zirconia with supported Pt, Ru, Ni, and Ni-Ru. *Top. Catal.* 56, 958–968. doi: 10.1007/s11244-013-0060-z

Bradford, M. C. J., and Vannice, M. A. (1998). CO_2 reforming of CH_4 over supported Pt catalysts. *J. Catal.* 173, 157–171. doi: 10.1006/jcat.1997.1910

Busto, M., Benitez, V. M., Vera, C. R., Grau, J. M., and Yori, J. C. (2008). Pt-Pd/WO3-ZrO2 catalysts for isomerization-cracking of long paraffins. *Appl. Catal. A* 347, 117–125. doi: 10.1016/j.apcata.2008.06.003

Busto, M., Grau, J. M., and Vera, C. R. (2010). Screening of optimal pretreatment and reaction conditions for the isomerization-cracking of long paraffins over Pt/WO_3-ZrO_2 catalysts. *Appl. Catal. A* 387, 35–44. doi: 10.1016/j.apcata.2010.07.061

Chai, J., Zhu, S., Cen, Y., Guo, J., Wang, J., and Fan, W. (2017). Effect of tungsten surface density of WO_3-ZrO_2 on its catalytic performance in hydrogenolysis of cellulose to ethylene glycol. *RSC Adv.* 7, 8567–8574. doi: 10.1039/C6RA27524A

Challiwala, M. S., Ghouri, M. M., Linke, P., El-Halwagi, M. M., and Elbashir, N. O. (2017). A combined thermo-kinetic analysis of various methane reforming technologies: comparison with dry reforming. *J. CO_2 Util.* 17, 99–111. doi: 10.1016/j.jcou.2016.11.008

Charisiou, N. D., Baklavaridis, A., Papadakis, V. G., and Goula, M. A. (2016b). Synthesis gas production via the biogas reforming reaction over Ni/MgO-Al_2O_3 and Ni/CaO-Al_2O_3 catalysts. *Waste Biomass Valorization* 7, 725–736. doi: 10.1007/s12649-016-9627-9

Charisiou, N. D., Papageridis, K. N., Siakavelas, S., Tzounis, L., Kousi, K., Baker, M. A., et al. (in press). Glycerol steam reforming for hydrogen production over nickel supported on alumina, zirconia and silica catalysts. *Top. Catal.* 1–25. doi: 10.1007/s11244-017-0796-y

Charisiou, N. D., Siakavelas, G., Papageridis, K. N., Baklavaridis, A., Tzounis, L., Avraam, D. G., et al. (2016a). Syngas production via the biogas dry reforming reaction over nickel supported on modified with CeO_2 and/or La_2O_3 alumina catalysts. *J. Nat. Gas Sci. Eng.* 31, 164–183. doi: 10.1016/j.jngse.2016.02.021

Charisiou, N. D., Siakavelas, G., Papageridis, K. N., Baklavaridis, A., Tzounis, L., Polychronopoulou, K., et al. (2017). Hydrogen production via the glycerol steam reforming reaction over nickel supported on alumina and lanthana-alumina catalysts. *Int. J. Hydrogen Energy* 42, 13039–13060. doi: 10.1016/j.ijhydene.2017.04.048

Chen, J., Wu, Q., Zhang, J., and Zhang, J. (2008). Effect of preparation methods on structure and performance of Ni/$Ce_{0.75}Zr_{0.25}O_2$ catalysts for CH_4-CO_2 reforming. *Fuel* 87, 2901–2907. doi: 10.1016/j.fuel.2008.04.015

Chen, Y.-Z., Liaw, B.-J., and Lai, W.-H. (2002). ZrO_2/SiO_2- and La_2O_3/Al_2O_3 supported platinum catalysts for CH_4/CO_2 reforming. *Appl. Catal. A* 230, 73–83. doi: 10.1016/S0926-860X(01)00996-6

Damyanova, S., Grange, P., and Delmon, B. (1997). Surface characterization of zirconia-coated alumina and silica carriers. *J. Catal.* 168, 421–430. doi: 10.1006/jcat.1997.1671

Damyanova, S., Pawelec, B., Arishtirova, K., and Fierro, J. L. G. (2012). Ni-based catalysts for reforming of methane with CO_2. *Int. J. Hydrogen Energy* 37, 15966–15975. doi: 10.1016/j.ijhydene.2012.08.056

Damyanova, S., Pawelec, B., Arishtirova, K., Huerta, M. V. M., and Fierro, J. L. G. (2009). The effect of CeO_2 on the surface and catalytic properties of Pt/CeO_2-ZrO_2 catalysts for methane dry reforming. *Appl. Catal. B* 89, 149–159. doi: 10.1016/j.apcatb.2008.11.035

Debecker, D. P., Gaigneaux, E. M., and Busca, G. (2009). Exploring, tuning, and exploiting the basicity of hydrotalcites for applications in heterogeneous catalysis. *Chemistry* 15, 3920–3935. doi: 10.1002/chem.200900060

Elsayed, N. H., Elwell, A., Joseph, B., and Kuhn, J. N. (2017). Effect of silicon poisoning on catalytic dry reforming of simulated biogas. *Appl. Catal. A* 538, 157–164. doi: 10.1016/j.apcata.2017.03.024

Fakeeha, A. H., Naeem, M. A., Khan, W. U., and Al-Fatesh, A. S. (2014). Syngas production via CO_2 reforming of methane using Co-Sr-Al catalyst. *J. Ind. Eng. Chem.* 20, 549–557. doi: 10.1016/j.jiec.2013.05.013

Ferreira, M. E. H., Moutinho, M. V. O., Stavale, F., Lucchese, M. M., Capaz, R. B., Achete, C. A., et al. (2010). Evolution of the Raman spectra from single, few, and many-layer graphene with increasing disorder. *Phys. Rev. B* 82:125429. doi: 10.1103/PhysRevB.82.125429

Gac, W. (2011). Acid-base properties of Ni-MgO-Al_2O_3 materials. *Appl. Surf. Sci.* 257, 2875–2880. doi: 10.1016/j.apsusc.2010.10.084

Gonzalez-DelaCruz, V. M., Ternero, F., Pereniguez, R., Caballero, A., and Holgado, J. P. (2010). Study of nanostructured Ni/CeO2 catalysts prepared by combustion synthesis in dry reforming of methane. *Appl. Catal. A* 384, 1–9. doi: 10.1016/j.apcata.2010.05.027

Goula, M. A., Bereketidou, O. A., Papageridis, K. N., and Charisiou, N. D. (2014). Influence of the preparation procedure parameters on the performance of Ni/g-alumina catalysts for the biogas reforming reaction. *WHEC* 3, 1435–1441.

Goula, M. A., Charisiou, N. D., Papageridis, K. N., Delimitis, A., Pachatouridou, E., and Iliopoulou, E. F. (2015). Nickel on alumina catalysts for the production of hydrogen rich mixtures via the biogas dry reforming reaction: influence of the synthesis method. *Int. J. Hydrogen Energy* 40, 9183–9200. doi: 10.1016/j.ijhydene.2015.05.129

Goula, M. A., Charisiou, N. D., Siakavelas, G., Tzounis, L., Tsiaoussis, I., Panagiotopoulou, P., et al. (2017). Syngas production via the biogas dry reforming reaction over Ni supported on zirconia modified with CeO_2 or La_2O_3 catalysts. *Int. J. Hydrogen Energy* 42, 13724–13740. doi: 10.1016/j.ijhydene.2016.11.196

Goula, M. A., Siakavelas, G., Papageridis, K. N., Charisiou, N. D., Panagiotopoulou, P., and Yentekakis, I. V. (2016a). Syngas production via the biogas dry reforming reaction over Ni supported on zirconia modified with CeO_2 or La_2O_3 catalysts. *WHEC,* 555–557.

Goula, M. A., Charisiou, N. D., Papageridis, K. N., and Siakavelas, G. (2016b). Hydrogen via the glycerol steam reforming reaction: influence of the synthesis method for Ni/Al_2O_3 catalysts. *Chin. J. Catal.* 37, 1949–1965. doi: 10.1016/S1872-2067(16)62518-4

Han, J. W., Park, J. S., Choi, M. S., and Lee, H. (2017). Uncoupling the size and support effects of Ni catalysts for dry reforming of methane. *Appl. Catal. B* 203, 625–632. doi: 10.1016/j.apcatb.2016.10.069

Iriondo, A., Cambra, J. F., Guemez, M. B., Barrio, V. L., Requies, J., Sanchez-Sanchez, M. C., et al. (2012). Effect of ZrO_2 addition on Ni/Al_2O_3 catalyst to produce H_2 from glycerol. *Int. J. Hydrogen Energy* 37, 7084–7093. doi: 10.1016/j.ijhydene.2011.11.075

Jafarbegloo, M., Tarlani, A., Mesbah, A. W., and Sahebdelfar, S. (2015). Thermodynamic analysis of carbon dioxide reforming of methane and its practical relevance. *Int. J. Hydrogen Energy* 40, 2445–2451. doi: 10.1016/j.ijhydene.2014.12.103

Kaniyoor, A., and Ramaprabhu, S. (2012). A Raman spectroscopic investigation of graphite oxide derived graphene. *AIP Adv.* 2:032183. doi: 10.1063/1.4756995

Kathiraser, Y., Oemar, U., Saw, E. T., Li, Z., and Kawi, S. (2015). Kinetic and mechanistic aspects for CO_2 reforming of methane over Ni based catalysts. *Chem. Eng. J.* 278, 62–78. doi: 10.1016/j.cej.2014.11.143

Kourieh, R., Bennici, S., Marzo, M., Gervasini, A., and Auroux, A. (2012). Investigation of the WO_3/ZrO_2 surface acidic properties for the aqueous hydrolysis of cellobiose. *Catal. Commun.* 19, 119–126. doi: 10.1016/j.catcom.2011.12.030

Kumar, P., Sun, Y., and Idem, R. O. (2007). Nickel-based ceria, zirconia, and ceria-zirconia catalytic systems for low-temperature carbon dioxide reforming of methane. *Energy Fuel* 21, 3113–3123. doi: 10.1021/ef7002409

Lehman, J. H., Terrones, M., Mansfield, E., Hurst, K. E., and Meunier, V. (2011). Evaluating the characteristics of multiwall carbon nanotubes. *Carbon* 49, 1581–1602. doi: 10.1016/j.carbon.2011.03.028

Li, W., Zhao, Z., and Jiao, Y. (2016). Dry reforming of methane towards CO^- rich hydrogen production over robust supported Ni catalyst on hierchically structured monoclinic zirconia nanosheets. *Int. J. Hydrogen Energy* 41, 17907–17921. doi: 10.1016/j.ijhydene.2016.07.272

Lovell, E., Jiang, Y., Scott, J., Wang, F., Suhardja, Y., Chen, M., et al. (2014). CO2 reforming of methane over MCM-41-supported nickel catalysts: altering support acidity by one-pot synthesis at room temperature. *Appl. Catal.* 473, 51–58. doi: 10.1016/j.apcata.2013.12.020

Luisetto, I., Tuti, S., Battocchio, C., Lo Mastro, S., and Sodo, A. (2015). Ni/CeO_2-Al_2O_3 catalysts for the dry reforming of methane: the effect of $CeAlO_3$ content and nickel crystallite size on catalytic activity and coke resistance. *Appl. Catal. A* 500, 12–22. doi: 10.1016/j.apcata.2015.05.004

Macht, J., and Iglesia, E. (2008). Structure and function of oxide nanostructures: catalytic consequences of size and composition. *Phys. Chem. Chem. Phys.* 10, 5331–5343. doi: 10.1039/b805251d

Martins, A. R., Carvalho, L. S., Reyes, P., Grau, J. M., and do Carmo Rangel, M. (2017). Hydrogen production on alumina-supported platinum catalysts. *J. Mol. Catal. A Chem*. 429, 1–9. doi: 10.1016/j.molcata.2016.11.040

Mustu, H., Yasyerli, S., Yasyerli, N., Dogu, G., Dogu, T., Djinovic, P., et al. (2016). Effect of synthesis route of mesoporous zirconia based Ni catalysts on coke minimization in conversion of biogas to synthesis gas. *Int. J. Hydrogen Energy* 40, 3217–3228. doi: 10.1016/j.ijhydene.2015.01.023

Ni, J., Chen, L., Lin, J., and Kawi, S. (2012). Carbon deposition on borated alumina supported nano-sized Ni catalysts for dry reforming of CH_4. *Nano Energy* 1, 674–686. doi: 10.1016/j.nanoen.2012.07.011

Nikoo, M. K., and Amin, N. A. S. (2011). Thermodynamic analysis of carbon dioxide reforming of methane in view of solid carbon formation. *Fuel Process. Technol.* 92, 678–691. doi: 10.1016/j.fuproc.2010.11.027

Oemar, U., Hidajat, K., and Kawi, S. (2015). Pd-Ni catalyst over spherical nanostructured Y_2O_3 support for oxy-CO_2 reforming of methane: role of surface oxygen mobility. *Int. J. Hydrogen Energy* 40, 12227–12238. doi: 10.1016/j.ijhydene.2015.07.076

Papageridis, K. N., Charisiou, N. D., Siakavelas, G., Avraam, D. G., Tzounis, L., Kousi, K., et al. (2016). Comparative study of Ni, Co, Cu supported on γ-alumina catalysts for hydrogen production via the glycerol steam reforming reaction. *Fuel Process. Technol*. 152, 156–175. doi: 10.1016/j.fuproc.2016.06.024

Phung, T. K., Hernández, L. P., and Busca, G. (2015). Conversion of ethanol over transition metal oxide catalysts: effect of tungsten addition on catalytic behavior of titania and zirconia. *Appl. Catal. A* 489, 180–187. doi: 10.1016/j.apcata.2014.10.025

Pompeo, F., Nichio, N. N., Souza, M. M. V. M., Cesar, D. V., Ferretti, O. A., and Schmal, M. (2007). Study of Ni and Pt catalysts supported on Al_2O_3 and ZrO_2 applied in methane reforming with CO_2. *Appl. Catal. A* 316, 175–183. doi: 10.1016/j.apcata.2006.09.007

Rezaei, M., Alavi, S. M., Sahebdelfar, S., Bai, P., Liu, X., and Yan, Z.-F. (2008). CO_2 reforming of CH_4 over nanocrystalline zirconia-supported nickel catalysts. *Appl. Catal. B* 77, 346–354. doi: 10.1016/j.apcatb.2007.08.004

Rhodes, M. D., and Bell, A. T. (2005). The effects of zirconia morphology on methanol synthesis from CO and H2 over Cu/ZrO_2 catalysts: part I. steady-state studies. *J. Catal*. 233, 198–209. doi: 10.1016/j.jcat.2005.04.026

Roh, H.-S., Platon, A., Wang, Y., and King, D. L. (2006). Catalyst deactivation and regeneration in low temperature ethanol steam reforming with Rh/CeO_2-ZrO_2 catalysts. *Catal. Lett*. 110, 1–6. doi: 10.1007/s10562-006-0082-2

Rouquerol, F., Rouquerol, J., and Sing, K. (1999). *Adsorption by Powders and Porous Solids*. Marseille: Academic Press.

Sarkar, D., Adak, S., Chu, M. C., Cho, S. J., and Mitra, N. K. (2007). Influence of ZrO2 on the thermo-mechanical response of nano-ZTA. *Ceram. Int*. 33, 255–261. doi: 10.1016/j.ceramint.2005.09.012

Sato, A. G., Volanti, D. P., Meira, D. M., Damyanova, S., Longo, E., and Bueno, J. M. C. (2013). Effect of the ZrO_2 phase on the structure and behavior of supported Cu catalysts for ethanol conversion. *J. Catal*. 307, 1–17. doi: 10.1016/j.jcat.2013.06.022

Shiju, N. R., AnilKumar, M., Hoelderich, W. F., and Brown, D. R. (2009). Tungstated zirconia catalysts for liquid-phase beckmann rearrangement of cyclohexanone oxime: structure-activity relationship. *J. Phys. Chem*. 113, 7735–7742. doi: 10.1021/jp810542t

Silveira, E. B., Rabelo-Neto, R. C., and Noronha, F. B. (2017). Steam reforming of toluene, methane and mixtures over Ni/ZrO_2 catalysts. *Catal. Today* 289, 289–301. doi: 10.1016/j.cattod.2016.08.024

Sing, K. S. W., Everett, D. H., Hall, R. A. W., Moscou, L., Pierotti, R. A., Rouquerol, J., et al. (1985). Reporting physisorption data for gas/solid systems with special reference to the determination of surface area and porosity. *IUPAC* 57, 603–619.

Sokolov, S., Kondratenko, E. V., Pohl, M. M., Barkschat, A., and Rodemerck, U. (2012). Stable low-temperature dry reforming of methane over mesoporous La_2O_3-ZrO_2 supported Ni catalyst. *Appl. Catal. B* 113–114, 19–30. doi: 10.1016/j.apcatb.2011.09.035

Sokolov, S., Kondratenko, E. V., Pohl, M. M., and Rodemerck, U. (2013). Effect of calcination conditions on time on-stream performance of Ni/La_2O_3-ZrO_2 in low-temperature dry reforming of methane. *Int. J. Hydrogen Energy* 38, 16121–16132. doi: 10.1016/j.ijhydene.2013.10.013

Sundaramurthy, V., Dalai, A. K., and Adjaye, J. (2008). The effect of phosphorus on hydrotreating property of NiMo/γ-Al_2O_3 nitride catalyst. *Appl. Catal. A* 335, 204–210. doi: 10.1016/j.apcata.2007.11.024

Sutthiumporn, K., and Kawi, S. (2011). Promotional effect of alkaline earth over Ni-La_2O_3 catalyst for CO_2 reforming of CH_4: role of surface oxygen species on H_2 production and carbon suppression. *Int. J. Hydrogen Energy* 36, 14435–14446. doi: 10.1016/j.ijhydene.2011.08.022

Taufiq-Yap, Y. H., Sudarno, Rashid, U., and Zainal, Z. (2013). CeO_2-SiO_2 supported nickel catalysts for dry reforming of methane toward syngas production. *Appl. Catal. A* 468, 359–369. doi: 10.1016/j.apcata.2013.09.020

Teterycz, H., Klimkiewicz, R., and Łaniecki, M. (2003). The role of Lewis acidic centers in stabilized zirconium dioxide. *Appl. Catal. A* 249, 313–326. doi: 10.1016/S0926-860X(03)00231-X

Theofanidis, S. A., Galvita, V. V., Poelman, H., and Marin, G. B. (2015). Enhanced carbon-resistant dry reforming Fe-Ni catalyst: role of Fe. *ACS Catal.* 5, 3028–3039. doi: 10.1021/acscatal.5b00357

Titus, J., Roussiere, T., Wasserschaff, G., Schunk, S., Milanov, A., Schwab, E., et al. (2016). Dry reforming of methane with carbon dioxide over NiO-MgO-ZrO_2. *Catal. Today* 270, 68–75. doi: 10.1016/j.cattod.2015.09.027

Torres, G. C., Manuale, D. L., Benítez, V. M., Vera, C. R., and Yori, J. C. (2012). Modification of the performance of WO_3-ZrO_2 catalysts by metal addition in hydrocarbon reactions. *Quim. Nova* 35, 748–754. doi: 10.1590/S0100-40422012000400018

Tsirka, K., Foteinidis, G., Dimos, K., Tzounis, L., Gournis, D., and Paipetis, A. S. (2017). Production of hierarchical all graphitic structures: a systematic study. *J. Colloid Interface Sci.* 487, 444–457. doi: 10.1016/j.jcis.2016.10.075

Usman, M., Wan Daud, W. M. A., and Abbas, H. F. (2015). Dry reforming of methane: influence of process parameters—a review. *Renew. Sustain. Energy Rev*. 45, 710–744. doi: 10.1016/j.rser.2015.02.026

Vasiliades, M. A., Makri, M. M., Djinovic, P., Erjavec, B., Pintar, A., and Efstathiou, A. M. (2016). Dry reforming of methane over 5wt% Ni/Ce1-xPrO2-δ catalysts: performance and characterization of active and inactive carbon by transient isotopic techniques. *Appl. Catal. B* 197, 168–183. doi: 10.1016/j.apcatb.2016.03.012

Velasquez, M., Batiot-Dupeyrat, C., Gallego, J., and Santamaria, A. (2014). Chemical and morphological characterization of multi-walled-carbon nanotubes synthesized by carbon deposition from an ethanol-glycerol blend. *Diamond Relat. Mater*. 50, 38–48. doi: 10.1016/j.diamond.2014.08.015

Wei, J., and Iglesia, E. (2004). Isotopic and kinetic assessment of the mechanism of reactions of CH_4 with CO_2 or H_2O to form synthesis gas and carbon on nickel catalysts. *J. Catal*. 224, 370–383. doi: 10.1016/j.jcat.2004.02.032

Xiang, X., Zhao, H., Yang, J., Zhao, J., Yan, L., Song, H., et al. (2016). Nickel based mesoporous silica-ceria-zirconia composite for carbon dioxide reforming of methane. *Appl. Catal. A* 520, 140–150. doi: 10.1016/j.apcata.2016.04.020

Yamaguchi, A., and Iglesia, E. (2010). Catalytic activation and reforming of methane on supported palladium clusters. *J. Catal*. 274, 52–63. doi: 10.1016/j.jcat.2010.06.001

Yentekakis, I. V., and Goula, G. (2017). Biogas management: advanced utilization for production of renewable energy and added-value chemicals. *Front. Environ. Sci.* 5:7. doi: 10.3389/fenvs.2017.00007

Yentekakis, I. V., Goula, G., Panagiotopoulou, P., Kampouri, S., Taylor, M. J., Kyriakou, G., et al. (2016). Stabilization of catalyst particles against sintering on oxide supports with high oxygen ion lability exemplified by Ir-catalyzed decomposition of N_2O. *Appl. Catal. B* 192, 357–364. doi: 10.1016/j.apcatb.2016.04.011

Yentekakis, I. V., Goula, G., Panagiotopoulou, P., Katsoni, A., Diamadopoulos, E., Matzavinos, D., et al. (2015). Dry reforming of methane: catalytic performance and stability of Ir catalysts supported on γ-Al_2O_3, $Zr_{0.92}Y_{0.08}O_2-\delta$ (YSZ) or $Ce_{0.9}Gd_{0.1}O_2-\delta$ (GDC) supports. *Top. Catal.* 58, 1228–1241. doi: 10.1007/s11244-015-0490-x

Yori, J. C., Pieck, C. L., and Parera, J. M. (1999). n-Butane isomerization on Pt/WO_3-ZrO_2: effect of the Pt incorporation. *Appl. Catal. A* 181, 5–14. doi: 10.1016/S0926-860X(98)00362-7

Youn, M. H., Seo, J. G., Jung, J. C., Park, S., Park, D. R., Lee, S. B., et al. (2009). Hydrogen production by auto-thermal reforming of ethanol over Ni catalyst supported on ZrO_2 prepared by a sol-gel method: effect of H_2O/P123 mass ratio in the preparation of ZrO_2. *Catal. Today* 146, 57–62. doi: 10.1016/j.cattod.2008.10.028

Yu, M., Zhu, Y. A., Lu, Y., Tong, G., Zhu, K., and Zhou, X. (2015). The promoting role of Ag in Ni-CeO_2 catalyzed CH_4-CO_2 dry reforming reaction. *Appl. Catal. B* 165, 43–56. doi: 10.1016/j.apcatb.2014.09.066

Zhao, W., Tan, P. H., Liu, J., and Ferrari, A. C. (2011). Intercalation of few-layer graphite flakes with $FeCl_3$: raman determination of fermi level, layer by layer decoupling, and stability. *J. Am. Chem. Soc.* 133, 5941–5946. doi: 10.1021/ja110939a

Zhao, X., Li, H., Zhang, J., Shi, L., and Zhang, D. (2016). Design and synthesis of NiCe@m-SiO_2 yolk-shell framework catalysts with improved coke-and sintering-resistance in dry reforming of methane. *Int. J. Hydrogen Energy* 41, 2447–2456. doi: 10.1016/j.ijhydene.2015.10.111

Zhou, W., Ross-Medgaarden, E. I., Knowles, W. V., Wong, M. S., Wachs, I. E., and Kiely, C. J. (2009). Identification of active Zr-WOx clusters on a ZrO_2 support for solid acid catalysts. *Nat. Chem.* 1, 722–728. doi: 10.1038/nchem.433

Conflict of Interest Statement: The authors declare that the research was conducted in the absence of any commercial or financial relationships that could be construed as a potential conflict of interest.